ENVIRONMENTAL EFFECTS ON CRACK GROWTH IN CONTINUOUS FIBER SIC-COMPOSITES

C. H. Henager, Jr., C. A. Lewinsohn, E. P. Simonen, and R. H. Jones

Pacific Northwest National Laboratory,*, Richland, WA 99352

ABSTRACT

A dynamic crack-growth model using discrete, two-dimensional fiber bridges developed for ceramic composites containing nonlinear, creeping fibers in an elastic matrix is used to develop a crack growth mechanism map. In addition to nonlinear creep, fiber oxidation and fiber/matrix interphase oxidation are treated and discussed. The model aids in the development of a crack-growth mechanism map based on available experimental crack growth data as a function of temperature and oxygen concentration and in terms of proposed crack-growth mechanisms; fiber relaxation (FR), interface removal (IR), viscous sliding (VS), oxidation embrittlement (OE), and fiber stress rupture (SR). Transitions between the various mechanisms are identified and discussed.

KEYWORDS

Dynamic crack growth, ceramic composites, mechanism map, modeling and simulation

INTRODUCTION

PNNL was among the first to identify and study time-dependent bridging in ceramic composites [1-3] and we have proposed a crack-growth mechanism map based on available experimental data as a function of temperature and oxygen partial pressure for continuous fiber composites with carbon interphases [4]. An approach to modeling dynamic time-dependent crack bridging has emerged from the work of Bückner [5] and Rice [6] based on the use of weight-functions to calculate crack-opening displacements [7]. Once a relationship [8,9] between crack-opening displacement and bridging tractions from crack-bridging elements is included, a governing integral equation obtains that relates the total crack opening, and the bridging tractions, to the applied load. The solution of this equation gives the force on the crack-bridges and the crack-opening displacement everywhere along the crack face [5-7,10]. Begley et al. [11] first developed a dynamic model and applied it to a variety of time-dependent bridging cases for linear creep laws [12-14]. Recently, a more appropriate bridging relation for creeping fibers has been developed by Cox et al.[9] that provides axial and radial stresses in creeping fibers with linear and non-linear creep laws.

* Pacific Northwest National Laboratory is operated for the U. S. Department of Energy by Battelle under Contract DE-AC06-76RLO 1830.

We have developed a similar bridging law for non-linear creeping fibers that also considers the case for interface removal due to oxidation. We treat discrete fiber bridges as opposed to a bridging force distribution and we employ a nonlinear (in time and stress) creep law to compute bridge extensions.

ENVIRONMENTAL EFFECTS: MODEL and MECHANISM MAP

Compliance of A Frictionally Bonded Fiber (Bridge)

We introduce an expression for the compliance of a bridging fiber, Φ_b, using the assumptions of frictional bonding with a weak, debonding interphase. The frictionally bonded fiber involves an unbonded or free length, l_{free}, and a debonded or frictionally bonded and sliding length, l_{deb}, for a fiber bridging a crack of opening u_t, as shown in Fig. 1.

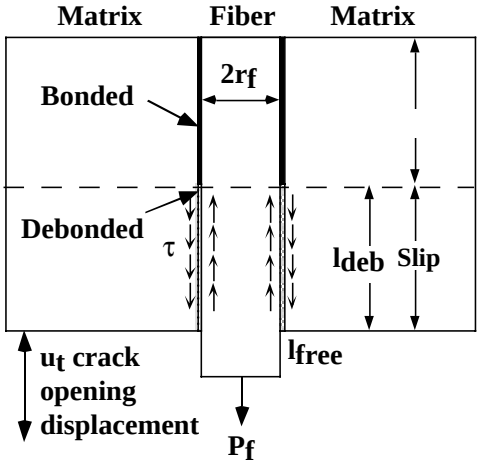

Figure 1. Schematic of frictionally bonded fiber acted upon by force P_f due to debonding and sliding across a Mode I crack with opening u_t. The lengths l_{deb} and l_{free} are shown.

The free length of fiber, which is not subject to frictional forces, is assigned a compliance, Φ_b^l, and the portion of the fiber subjected to a frictional sliding resistance along length l_{deb} due to P_f is assigned a nonlinear compliance, $\Phi_f{}^n$, such that $\delta_b = \Phi_b' P_b + \Phi_b'' P_b^2$ [15], where P_b is the 2D normalized bridge force and δ_b is the bridge displacement. As suggested by Cox et al. [9] one could include a time-dependent debonding from fiber contraction due to Poisson effect and creep deformation, which provides an additional time-dependent fiber compliance term.

Fiber Relaxation due to Creep (FR)

The time-dependent extension of a fiber bridge at elevated temperatures obeys a power-law creep equation [16] for Nicalon-CG and Hi-Nicalon fibers as

$$\varepsilon_f = A\sigma^n t^p \exp\left(\frac{-pQ}{RT}\right) = C(T)\sigma^n t^p \Rightarrow \dot{\varepsilon}_f = C(T)\sigma^n p t^{p-1} \tag{1}$$

where A is a constant, t is time, Q is an activation energy for creep, R and T have their usual meanings, n is the stress exponent, and p is the time-temperature exponent. The unbonded length given by l_{free} creeps at the bridging stress applied to the fiber. The debonded length of the fiber creeps at a stress that varies over the debond length, which is found by integration. The creep extension of a bridge becomes

$$\Delta l_{free} = C(T) p t^{p-1} \Delta t \left(\frac{P_b}{2r_f}\right)^n l_{free} \tag{2}$$

for the free length of fiber and

$$\Delta l_{deb} = C(T)pt^{p-1}\Delta t\int_0^{l_{deb}} \sigma^n(z)dz = C(T)pt^{p-1}\Delta t\left(\frac{P_b}{2r_f}\right)^n l_{deb}\left(1-\frac{1}{(1+\xi)^n 1+n}\right) \quad (3)$$

for the debonded length when the axial fiber stress is given by

$$\sigma(z) = \frac{P_b}{2r_f} - \frac{2\tau z}{r_f} \quad (4)$$

where t is the total creep time, Δt is the time step, and z is the axial distance along the fiber measured from the crack face. Time, t, is referenced to the inception of each bridge into the bridging zone and is tracked separately for each bridge.

Fiber/Matrix Interphase Removal by Oxidative Volatilization (IR)

When the fiber/matrix interphase is a material that can undergo a gaseous reaction with oxygen then interphase removal in oxygen-containing environments becomes important. Previous research has shown that the following interphase recession data applies to the typical 0/90 plain weave CVI-SiC/SiC_f materials with a CVI carbon interphase [17]

$$l_{ox} = 3.3\times10^{-4}e^{-6014/T}P_{O2}{}^{0.889}t = R(T,P_{O2})t \text{ thus } \Delta l_{ox} = R(T,P_{O2})\Delta t \quad (5)$$

where l_{ox} is the recession distance along the fiber/matrix interphase from the crack face into the composite in m/s, T is temperature in K, P_{O2} is fractional oxygen concentration, and t is exposure time. We assume that l_{deb} is maintained at its value determined by τ and the load on the fiber.

Oxidation of the Bridging Fiber (OE and VS/OE)

Exposed bridging fibers will undergo oxidation at elevated temperatures according to [18]

$$fib_{ox} = 1.84\times10^{-7}e^{-4016.8/T}P_{O2}t^{0.5} \quad (6)$$

where fib_{ox} is the oxide thickness grown on the fiber in m, T is temperature in K, P_{O2} is fractional oxygen concentration, and t is exposure time in s.

Fiber Stress Rupture (SR)

Exposed bridging fibers will obey time-dependent stress rupture relationships as [19]

$$\text{Ln}(\sigma_f) = 2.3E - (\beta/R)\left[RT(\text{Ln}(t)+C)\right] \quad (7)$$

where σ_f is fiber strength in MPa, and E, β, and C are fitted parameters from single fiber rupture tests in air.

Crack Growth Mechanism Map

The proposed mechanism map is shown in Fig. 2. Fiber creep relaxation (FR) dominates at high temperatures and low oxygen concentrations, as expected, since creep activation energies are high (~ 600 kJ/mol) and oxidation activation energies are low (~ 50 kJ/mol). Crack extension is dominated by interface removal (IR) for oxygen concentrations less than ~ 0.1 when the temperatures are not extreme. We observe both kinetic and activation energy changes in our experimental data consistent with this hypothesis. We define the transition from FR to IR by the locus of points where the crack growth from each mechanism is equal. At higher oxygen concentrations, the fiber/matrix interphase oxidizes and is replaced by a glass phase

and either oxidation embrittlement (OE) or viscous sliding (VS) mechanisms may occur. We propose that interphase glass formation and channel pinch-off (fiber-matrix bonding) at intermediate temperatures where the resultant glass phase is brittle results in OE and the fibers fail since they can no longer slide relative to the matrix. We define the transition from IR to OE as the locus of points where the fiber/matrix channel pinches-off and OE occurs in a finite crack growth increment (2.5 mm in this case). At higher temperatures the glass phase is viscous, not brittle and VS occurs. When the glass phase has a high viscosity, fibers can fail by rupture since the local fiber/matrix bonding leads to stress concentrations [20], rather like replacing an interface with a low frictional sliding stress with a higher one. It follows that there will be a temperature above which this stress concentration will not fail the fibers but this will depend on the details of the compositionally dependent glass viscosity. The transition from OE to VS/OE is schematic since we do not yet know the glass viscosity nor have we implemented a viscous sliding treatment for the model, although such treatments exist [21]. Fiber oxidation also results in loss of strength, which leads to embrittlement via fiber stress rupture (SR) [16,22,23]. Fiber stress corrosion should be accounted for by the SR mechanism since this data was obtained in air. Since predicted fiber stresses in the crack wake of a dynamic crack are on the order of 800 MPa or smaller, SR is difficult to achieve until temperatures above about 1400K.

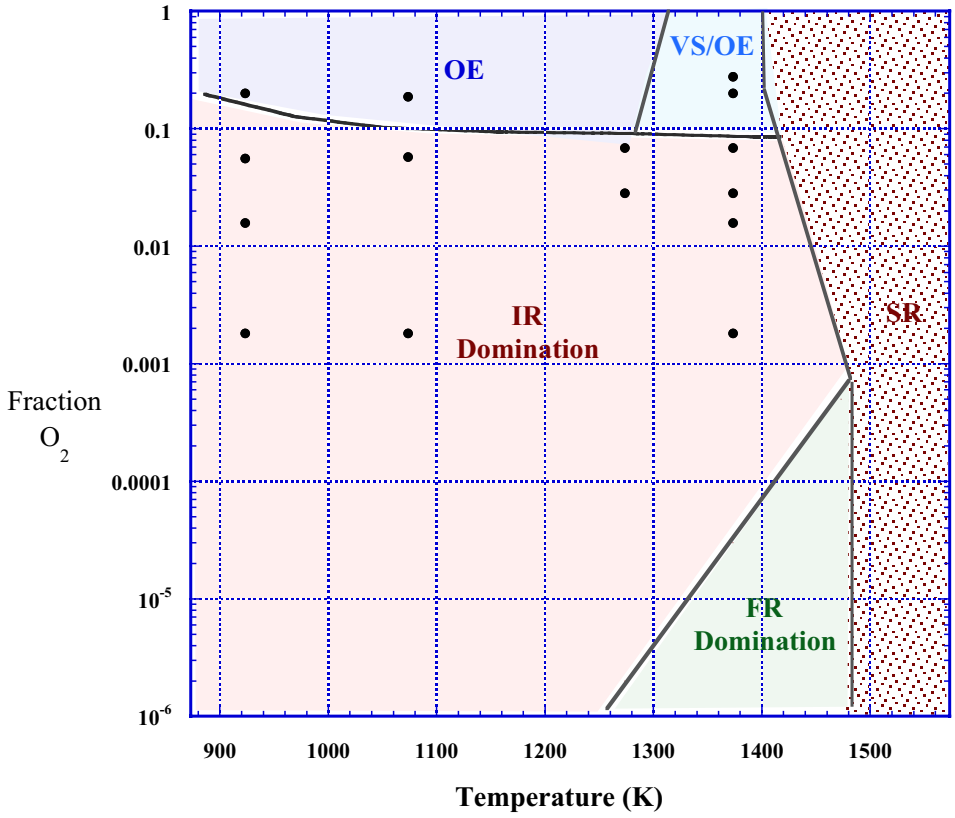

Figure 2. Suggested dominant crack growth mechanisms based on experimental data and model results. The plotted points correspond to experiments with Nicalon-CG composites and the map is fashioned using data appropriate for Nicalon-CG fibers.

DISCUSSION

The materials included in the map, and indicated by the plotted points (Fig. 2) are 2D woven SiC/SiC composites with Nicalon-CG fibers at ~ 40% by volume. Lewinsohn et al. [4] discuss the map concept, the materials, and the experimental data more fully. However, we have observed that temperature and oxygen concentration play the most important roles in determining the operable crack growth mechanisms.

Therefore, it was imperative to include oxidation in the dynamic crack model in addition to the nonlinear fiber creep. However, additional modeling remains and more experimentation is planned.

Crack growth appears to be controlled by FR above the composite matrix-cracking threshold at elevated temperatures in inert environments. PNNL and others have determined composite deformation rates[1,2,24-35] and activation energies under these conditions and they match quite well with activation energies for fiber creep, about 500 – 600 kJ/mol. Our dynamic crack growth model agrees reasonably well with measured crack growth rates and these activation energies.

When oxygen is introduced during the crack growth testing the deformation rates increase and the activation energy decreases to about 50 kJ/mol, in agreement with carbon oxidation processes. Significantly, the crack growth kinetics change from nonlinear to linear since now the bridge compliance is dominated by the linear portion as $l_{free} + l_{ox}$ approach and exceed l_{deb}. Again, our model agrees well with these changes in both kinetics and activation energies. The transition between the FR and IR mechanisms is defined as the locus of points where the crack growth rates of each mechanism are roughly equal. This was determined by choosing an oxygen concentration where the crack velocity doubled compared to the velocity without any oxygen. This curve is steep as shown in Fig. 2 due in part to the high activation energy of the fiber creep process. It is bounded at high temperatures by fiber stress rupture mechanisms.

Transitions from IR to either OE or VS/OE mechanisms are shown. We find that there is a competition between specimen failure due to IR relative to the time for pinch-off and OE to occur. The dynamics are handled by removing those fibers from the bridging zone that have an oxide thickness greater than some critical value, such as the interphase thickness. However, this transition is crack length (specimen size) and interphase thickness dependent. The size effect occurs since OE depends on total fiber exposure time, which is dependent on crack length. Interphase thickness effects arise due to our criterion that pinch-off occurs prior to the onset of OE. The computations shown here are for an interphase thickness of 150 nm. Other plausible OE mechanisms only require a critical oxide thickness that is not interphase thickness dependent [36,37]. However, such mechanisms will still exhibit a specimen size effect or history effect. Transitions from OE (pinch-off with brittle glass phase) to VS/OE (non-brittle, viscous glass phase) depend on the viscosity of the glass which is strongly dependent on glass composition. Thus, these transitions are not rigorously defined here and will have to wait for future work. By incorporating existing models of viscous interphase mechanics, we will be able to understand the effects of viscosity on fiber stress concentrations.

The database for fiber stress rupture is mainly limited to tests in air so dependence on oxygen concentration is lacking. SR competes with OE and IR at temperatures higher than about 1373K for oxygen concentrations near 0.2 The onset of SR occurs at 1373K in air during dynamic crack growth according to our model and this onset is predicted to shift to 1423K for lower oxygen concentrations. Without detailed data as a function of oxygen concentration, we cannot be more quantitative. The map suggests that SR shifts to higher temperatures as the oxygen concentration decreases. The boundary between FR and SR is suggested to occur at the fiber thermal limits. There is a need for additional stress rupture data as a function of oxygen concentration.

SUMMARY

We developed a dynamic crack-growth model with the following features: 1) it is based on the weight-function method using discrete fiber bridges, 2) it contains nonlinear bridge extension laws based on fiber-creep kinetics for Nicalon-CG and Hi-Nicalon fibers, 3) it contains bridge extension laws for the case of interphase removal, and 4) it provides fully dynamic crack tracking using a critical-stress-intensity propagation criterion. The model reproduces the time-dependent crack-growth kinetics observed

experimentally in specimens of Nicalon-CG and Hi-Nicalon 0/90 woven composites. The transition from nonlinear crack growth kinetics to linear growth kinetics is also reproduced by the model by comparing crack growth rates under FR or IR domination. By implementing a simple "fiber removal" algorithm, where the criterion for removal is based either on a critical oxide thickness or stress rupture threshold, we can also map out transitions between crack growth due to OE and SR. The model is useful in helping us develop and understand crack growth mechanisms and to design improved composite materials.

REFERENCES

1. C. H. Henager, Jr. and R. H. Jones, *Mater. Sci. Eng., A*, 1993, **A166** 211.
2. C. H. Henager, Jr. and R. H. Jones, *J. Am. Ceram. Soc.*, 1994, **77** 2381.
3. C. H. Henager, Jr., R. H. Jones, C. F. Windisch, Jr., M. M. Stackpoole, and R. Bordia, *Metall. Mater. Trans. A*, 1996, **27A** 839.
4. C. A. Lewinsohn, C. H. Henager, Jr., and R. H. Jones, *Ceram. Trans.*, 1999, **96** 351.
5. H. Bückner, *Z. Angew Math. Mech.*, 1970, **46** 529.
6. J. R. Rice, *Int. J. Solids Struct.*, 1972, **8** 751.
7. T. Fett, C. Mattheck, and D. Munz, *Engr. Fract. Mech.*, 1987, **27** 697.
8. D. B. Marshall, B. N. Cox, and A. G. Evans, *Acta Metall.*, 1985, **33** 2013.
9. B. N. Cox, N. Sridhar, and C. R. Argento, *Acta Mater.*, 2000, **48** 4137.
10. B. N. Cox and D. B. Marshall, *Acta Metall. Mater.*, 1991, **39** 579.
11. M. R. Begley, B. N. Cox, and R. M. McMeeking, *Acta Metall. Mater.*, 1995, **43** 3927.
12. M. R. Begley, A. G. Evans, and R. M. McMeeking, *J. Mech. Phys. Sol.*, 1995, **43** 727.
13. M. R. Begley, B. N. Cox, and R. M. McMeeking, *Acta Metall. Mater.*, 1997, **45** 2897.
14. B. N. Cox, D. B. Marshall, R. M. McMeeking, and M. R. Begley, *Solid Mech. Appl.*, 1997, **49** 353.
15. C. H. Henager, Jr. and R. G. Hoagland, *Ceramic Trans.*, 2001, **124** 315.
16. J. A. DiCarlo, *Ceramurgia*, 1998, **28** 88.
17. C. F. Windisch, Jr., J. Charles H. Henager, G. D. Springer, and R. H. Jones, *J. Am. Ceram. Soc.*, 1997, **80** 569.
18. Y. T. Zhu, S. T. Taylor, M. G. Stout, D. P. Butt, and T. C. Lowe, *J. Am. Ceram. Soc.*, 1998, **81** 655.
19. J. A. DiCarlo, H. M. Yun, G. N. Morscher, and J. C. Goldsby, *Ceram. Trans.*, 1995, **58** 343.
20. W. H. Glime and J. D. Cawley, *J. Am. Ceram. Soc.*, 1998, **81** 2597.
21. S. V. Nair, K. Jakus, and T. J. Lardner, *Mech. Mater.*, 1991, **12** 229.
22. H. M. Yun and J. A. DiCarlo, *Ceram. Trans.*, 1996, **74** 17.
23. R. E. Tressler and J. A. DiCarlo, *Ceram. Trans.*, 1995, **57** 141.
24. F. Abbe, J. Vicens, and J. L. Chermant, *J. Mater. Sci. Lett.*, 1989, **8** 1026.
25. J. L. Chermant, F. Abbe, and D. Kervadec, *Creep Fract. Eng. Mater. Struct., Proc. Int. Conf., 5th*, , 1993, 371.
26. X. Wu and J. W. Holmes, *J. Am. Ceram. Soc.*, 1993, **76** 2695.
27. G. Grathwohl, B. Meier, and P. Wang, *Key Eng. Mater.*, 1995, **108-110** 243.
28. A. G. Evans and C. Weber, *Mater. Sci. Eng., A*, 1996, **A208** 1.
29. D. R. Mumm, W. Morris, M. S. Dadkhah, and B. N. Cox, *ASTM Spec. Tech. Publ.*, 1997, **STP 1309** 102.
30. M. Mizuno, S. Zhu, Y. Kagawa, and H. Kaya, *Key Eng. Mater.*, 1997, **132-136** 1942.
31. B. Cox and F. Zok, *Brittle Matrix Compos. 5, Proc. Int. Symp., 5th*, , 1997, 487.
32. B. Wilshire, F. Carreno, and M. J. L. Percival, *Scr. Mater.*, 1998, **39** 729.
33. J.-L. Chermant and G. Boitier, *Adv. Compos. Mater.*, 1999, **8** 77.
34. S. Zhu, M. Mizuno, Y. Kagawa, J. Cao, Y. Nagano, and H. Kaya, *J. Am. Ceram. Soc.*, 1999, **82** 117.
35. R. E. Tressler, K. L. Rugg, C. E. Bakis, and J. Lamon, *Key Eng. Mater.*, 1999, **164-165** 297.
36. A. G. Evans, F. W. Zok, R. M. McMeeking, and Z. Z. Du, *J. Am. Ceram. Soc.*, 1996, **79** 2345.
37. F. E. Heredia, J. C. McNulty, F. W. Zok, and A. G. Evans, *J. Am. Ceram. Soc.*, 1995, **78** 2097.